First-principles calculations of tetragonal FeX (X = S, Se, Te): magnetism, hyperfine-interaction, and bonding

V. Koteski[a], V.N. Ivanovski[a,*], A. Umićević[a], J. Belošević-Čavor[a], D. Toprek[a], H.-E. Mahnke[b,c]

[a] *Vinča Institute of Nuclear Sciences, University of Belgrade, Serbia*
[b] *Freie Universität Berlin, Fachbereich Physik*
[c] *Helmholtz-Zentrum Berlin, Germany*

Abstract

Magnetic ground states, local crystallographic environment of Fe, and hyperfine interaction parameters in tetragonal FeX (X = S, Se, Te) are investigated by means of density functional theory (DFT) calculations using augmented plane waves plus local orbitals (APW+lo) method. We use several different magnetic configurations to evaluate the magnetic and electronic properties of this system, as well as the hyperfine interaction parameters at Fe lattice site. The results obtained for the ground state collinear anti-ferromagnetic arrangement relatively well reproduce the quadruple splitting and isomer shifts from the available Mössbauer measurements. The Bader's atoms in molecule charge density analysis indicates bonding of closed-shell type and a sizable charge transfer from Fe to X. The system properties are sensitive to the structural optimization of the position of the chalcogen atom with respect to the iron plane.

Keywords: local density approximation, Mössbauer effect, superconductors
PACS: 71.15.Mb, 76.80.+y, 74.25.-q

*Corresponding author
Email address: valiva@vin.bg.ac.rs (V.N. Ivanovski)

1. Introduction

Tetragonal FeX (X = S, Se, Te) belong to the class of iron-based superconductors with layered structure. The unconventional properties of these Fe-chalcogenides have recently attracted a lot of research interest [1–6]. This is related to the still not yet understood interplay between superconductivity and magnetism. The fact that the iron atom is important for coexistence of superconductivity and magnetism has also initiated several Mössbauer studies [7–9]. Mössbauer spectroscopy is a locally sensitive experimental method for probing the electronic and magnetic environment around the Fe ions. In essence, these studies have found no measurable hyperfine magnetic field at the Fe lattice site, and a relatively low quadrupole splitting with a weak temperature dependence.

The itinerant nature of the spin fluctuations in tetragonal FeX has been proposed as one of the mechanisms of high-temperature superconductivity that would also explain the lack of measurable magnetic field in a typical Mössbauer experiment [10].

It is clear that the electronic structure of these materials is important for understanding of their properties. Whereas there are several ab-initio density functional theory (DFT) studies [11–14] dealing with the structural, magnetic, and electronic properties of these materials, to our knowledge, there are no systematic calculations of the hyperfine-interaction (HI) parameters and properties of the local charge distribution and chemical bonds.

Here we present DFT calculations of the electronic structure, magnetic properties, finally yielding HI parameters, and local bonding in the tetragonal FeS, FeSe, and hypotetical pure FeTe. The magnetic calculations were performed assuming ferromagnetic, checkerboard anti-ferromagnetic, and collinear-anti-ferromagnetic configurations. The bi-collinear magnetic order was also checked as a possible magnetic ground state of FeTe. Here, one takes into account the fact that only tetragonal $Fe_{1+y}Te$ occurs in nature.

There is a relatively good agreement between the calculated and experimental HI parameters, especially considering the trends across the investigated

systems. This could indicate that excess interstitial Fe does not have significant influence on HI parameters and local bonding. We used both the experimental and the optimized lattice parameters to test the effects of optimization on the locally sensitive parameters. We found that nearly all calculated properties are sensitive to the value of the internal parameter u (i.e., the displacement of the chalcogen atom out of the iron plane).

In contrast to the Mössbauer spectroscopy experiments, our calculations show that, locally, there are sizable hyperfine magnetic fields ($B_{\rm hf}$). This is not unexpected, and in agreement with the other available theoretical studies that also predict sizable Fe magnetic moments. The chemical bonds between the atoms are found to be of closed-shell type.

2. DFT Calculations

To calculate the electronic structure of FeX (X = S, Se, Te), we employed the all-electron Wien2k code [15] based on the density functional theory (DFT) and the augmented plane wave (APW) plus local orbitals (lo) scheme. The Wien2k code is one of the most accurate codes [16] available for performing ab-initio calculations in solids. FeS, FeSe, and FeTe have a very simple structure (see Figure 1). The iron atoms are at the ($2a$), while the chalcogen atoms are at the ($2c$) Wyckoff position.

Muffin-tin spheres of 2.17, 1.77, 1.97, and 2.17 a.u. were chosen for Fe, S, Se, and Te respectively. To relax the internal atomic position of the anions in the tetragonal FeX (X = S, Se, Te) structure (space group $P4/nmm$) and to obtain all ground state properties of interest here we used a k-point grid of 15×15×11 points. Equivalent grids were used for the magnetic calculations that required larger unit cells (Figure 1). The RK_{max} parameter, which determines the size of the basic set, was set to 8.5 for all calculations. The self-consistent charge convergence criterion was 5×10^{-5}. The maximum force between atoms was converged to less than 0.025 eVÅ^{-1}.

In the Wien2k code, the electric field gradient (EFG) tensor is obtained

by solving the Poisson's equation directly from the non-spherical charge density [17]. The Mössbauer isomer shift (δ) are evaluated from the self-consistent electron density using the procedure described in Ref. [18]. Without orbital magnetism, the dominant contribution to the hyperfine fields comes from the Fermi contact term, which is determined in scalar-relativistic calculations from the spin density at the nucleus [19, 20].

Following the approach of Mazin et al. [12], both the standard local (spin) density approximation [L(S)DA] and the gradient corrected (GGA) implementation [21] to the LDA were used. The LDA is known to describe the magnetic details of itinerant magnetic systems more accurately, whereas the GGA gives better results for structural optimization. Therefore, the structural parameters in our calculations were obtained by using the GGA approximation in the non-magnetic case. This is the closest approximation to the experimentally determined paramagnetic state. With the optimized parameters, we then switch to LDA calculations to obtain the hyperfine interaction [22], magnetic and electronic properties of the system.

We considered several magnetic orderings: non-magnetic (NM), ferromagnetic (FM), checkerboard anti-ferromagnetic (AFM1), and collinear anti-ferromagnetic (AFM2) (see Figure 1). Along the z axis, the FeX layers are held together by weak van der Waals forces. Because of the van der Waals interaction, it is not possible to determine the total energy minimum along this axis within the DFT formalism. Hence, the optimization of the c lattice parameter was not included.

For each of the magnetic states, we examined two scenarios: (i) a, c, and u (internal parameter) fixed to their corresponding experimental values and (ii) a and u optimized from NM GGA calculations, with c fixed to its experimental value. To obtain the optimized geometry in the $x-y$ plane, the total energy was calculated for a set of a values between +4 and -4 % of the experimental lattice parameter. Before as well as after the optimization of a, we relaxed the only internal degree of freedom in this structure, u, which is the z-coordinate of the anions. This step was found to be crucial, because optimizing a without a previously optimized u gives values too far away from the experimental a

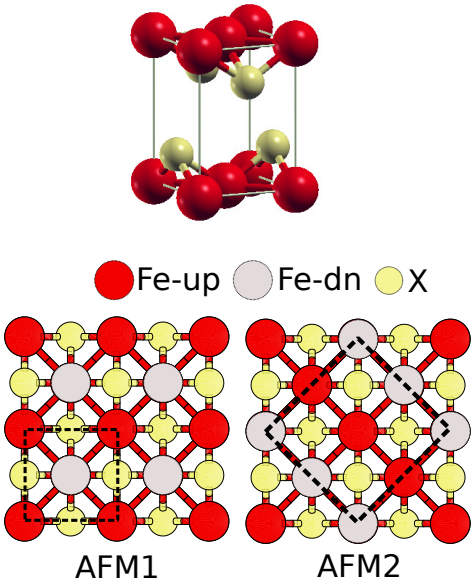

Figure 1: (Color online) Tetragonal unit cell of FeX (X = S, Se, Te) (top), along with a top view of the checkerboard anti-ferromagnetic (AFM1), and collinear anti-ferromagnetic (AFM2) order (bottom). The dashed lines denote the corresponding unit cells used in the calculations. The upper image is obtained by using the XCRYSDEN visualization program [23].

Table 1: Total energy differences (ΔE in meV/f.u.) for different magnetic configurations of FeS, FeSe, and FeTe. The results are given with respect to the NM energy, set to 0. The theoretical lattice parameters are obtained from GGA NM calculations with experimental c value (see text).

	GGA			LDA		
	FM	AFM1	AFM2	FM	AFM1	AFM2
ΔE FeS-exp.	0	-50	-79	0	-4	-21
ΔE FeS-theor.	0	+0.001	-2.3	0	-0.001	-0.08
ΔE FeSe-exp.	+42.2	-168.5	-210.8	-0.2	-74.8	-104.2
ΔE FeSe-theor.	0	-27.7	-53.4	0	+0.3	-14.0
ΔE FeTe-exp.	-295.9	+477.1	-336.6	-168.8	-156.5	-220.1
ΔE FeTe-theor.	-8.3	+665.2	-120.4	-0.8	-26.3	-57.7.0

parameter.

3. Ground State Magnetic Configuration

The difference in total energy calculated for the various magnetic configurations is given in Table 1. ΔE denotes the total energy in meV per formula unit (f.u.) relative to the energy of the NM state, set to 0. We see that the AFM2 state is the magnetic ground state of all three systems within theoretical framework we considered. The AFM2 state has the largest magnetic stabilization energy when either experimental or theoretical parameters are used. AFM2 is also the ground state regardless of the functional used. This state consists of alternating stripes of parallel Fe spins coupled antiferromagnetically to one another.

This agrees well with the DFT study of FeS based on a plane-wave basis set and ultrasoft pseudopotentials by Kwon et al. [11]. The collinear-ordered FeSe state was also found to be the ground state of this system in other DFT calculations [13, 14].

For FeTe, however, Ma et al. [14] found that the bi-collinear state is ener-

getically more favorable (by 10 meV/f.u.) than the collinear state. They used a plane-wave basis set method, the same PBE flavor of the GGA approximation as in our case, and lattice parameters fixed to the experimental values.

After testing the bi-collinear state in the experimental and theoretical geometries, we found that this state has higher energy by 38, 12, and 42 meV/f.u. than the collinear configuration when using the LDA theoretical, LDA experimental, and GGA theoretical parameters, respectively. Interestingly, only when the experimental lattice parameters are used in combination with the GGA approximation (as in Ref. [14]), the bi-collinear state is the magnetic ground state of FeTe (lower in energy by 6 meV).

Our calculations show that for FeS and FeSe, the bi-collinear state always has higher energy than the collinear magnetic arrangement in both optimization scenarios. In fact, for FeS, taking into account all the different magnetic configurations considered here, including the NM case, the bi-collinear state has always the highest total energy.

The FeS and FeSe tetragonal structures cannot sustain the ferromagnetic ordering, with the Fe atoms barely retaining any magnetic moment at all. For these systems, the FM state essentially converges to the NM state regardless of optimization scheme used. In contrast, FeTe has a stable FM ordering with sizable stabilization energy. On the other hand, the stability of the checkerboard AFM1 state strongly depends on the system in question, the value of the structural parameters, and functional type.

Experimental work has confirmed the absence of long range magnetic order in tetragonal FeSe [24, 25]. This is also the case for tetragonal FeS where the local probe muon spin resonance measurements only found coexistence of superconductivity with small moment ($(10^{-2}$ - $10^{-3})$ μ_{B}) magnetism from the impurity phase [4]. $Fe_{1+y}Te$ features bicollinear AFM order [26, 27].

4. Structural properties, magnetism, and hyperfine-interaction parameters

4.1. HI parameters and Magnetic Ordering

The calculated HI parameters strongly depend on the type of magnetic ordering and functional of the electron density. To illustrate this, in Figure 2 we show the hyperfine fields, $B_{\rm hf}$, electric field gradients, V_{zz}, and chemical shifts ($\delta_{\rm CS}$), as a function of the different magnetic arrangements in the LDA and GGA approximation. The hyperfine magnetic field increases its value when going from left to right, following the trend of the increasing Fe magnetic moments (not shown here). The electric field gradients in FeS seem to be relatively flat with respect to the magnetic ordering and functional used, but the same cannot be said about their values in FeSe and FeTe. The chemical shifts are only slightly dependent on the type of magnetic ordering.

In the following we will turn out attention to the structural, magnetic and HI parameters as calculated within the LDA approximation in the collinear AFM2 magnetic ground state. We will use these results, as obtained in the experimental and optimized geometries, to compare with the available experimental results. As already indicated, the LDA approximation was used as it is believed to more accurately describe the properties of the itinerant magnetic systems [12].

4.2. Collinear Anti-ferromagnetic Ground State

4.2.1. Geometry Optimization

Our relaxation procedure gives theoretical a values very close to the experimental lattice parameters (0.8% deviation for FeS, 0.9% for FeSe, and 0.1% for FeTe). There is a much larger deviation of the calculated u parameter, however, with the theoretical Fe-X nearest neighbor (NN) distances underestimated by 0.3% for FeS, overestimated by 2.2% for FeSe, and underestimated by 4.4% for FeTe.

The symmetry of the unit cell is such that there are no forces acting on the Fe ions. Consequently the Fe-Fe second neighbor (NNN) distances, $d_{\rm Fe-Fe}$, are determined from the value of the lattice parameter a only.

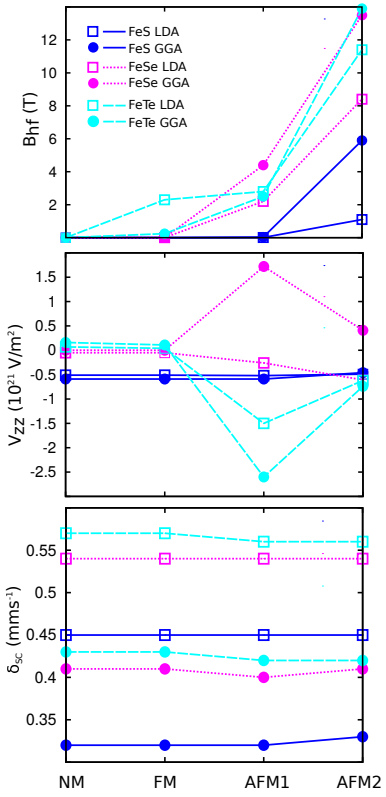

Figure 2: (Color online) Hyperfine fields, $B_{\rm hf}$, electric field gradients, V_{zz}, and chemical shifts, $\delta_{\rm CS}$, at Fe lattice site in tetragonal FeS, FeSe, and FeTe. The theoretically optimized lattice parameters were used. NM, FM, AFM1, and AFM2 denote the non-magnetic, ferromagnetic, checkerboard anti-ferromagnetic, and collinear anti-ferromagnetic states, respectively.

Table 2: Calculated structural, magnetic, and HI parameters of FeS, FeSe, and FeTe within the LDA approximation: (*i*) a, c, and u fixed to the experimental values; (ii) a and u optimized from NM GGA calculations, c fixed to the corresponding experimental value. In all cases the AFM2 magnetic ground state configuration was assumed.

(i) WIEN2k calculations with experimental lattice parameters a, c, and u			
	FeS	FeSe	FeTe
a	3.674[a]	3.771[b]	3.825[c]
c	5.023[a]	5.522[b]	6.291[c]
u	0.260[a]	0.267[b]	0.279[c]
$d_{\mathrm{Fe-S}}$	2.184	2.393	2.596
$d_{\mathrm{Fe-Fe}}$	2.598	2.667	2.705
$\lvert\mu_{\mathrm{Fe}}\rvert$ (μ_{B})	1.16	1.87	2.10
B_{hf} (T)	10.0	15.1	15.6
V_{zz} (10^{21} Vm^{-2})	-0.45	0.51	0.99
η	0.8	0.36	0.52
δ_{CS} (mms^{-1})	0.55	0.62	0.61
(ii) WIEN2k calculations with theoretical lattice parameters a and u			
	FeS	FeSe	FeTe
a	3.643	3.737	3.828
c	5.023[a]	5.522[b]	6.291[c]
u	0.237	0.245	0.252
$d_{\mathrm{Fe-}X}$	2.178	2.446	2.483
$d_{\mathrm{Fe-Fe}}$	2.576	2.761	2.707
$\lvert\mu_{\mathrm{Fe}}\rvert$ (μ_{B})	0.14	0.95	1.39
B_{hf} (T)	1.3	8.4	11.4
V_{zz} (10^{21} $\mathrm{V/m}^{2}$)	-0.49	-0.62	-0.62
η	0.02	0.85	0.48
δ_{CS} (mms^{-1})	0.45	0.54	0.56

[a]Experimental value from Ref. [28]

[b]Experimental value from Ref. [29]

[c]Experimental value from Ref. [30]

4.2.2. Magnetism

Table 2 summarizes the calculated magnetic and hyperfine interaction parameters. We see two clear trends: the iron magnetic moments, μ_{Fe}, and the hyperfine fields, B_{hf}, increase along the sequence FeS→FeSe→FeTe, while the structural optimization brings these values systematically down.

The calculated LDA Fe magnetic moment in FeS without structural optimization of 1.16 μ_{B} is in very good agreement with the averaged itinerant spin fluctuations experimental estimate of 1 μ_{B} [11]. In the optimization, μ_{Fe} is reduced to 0.14 μ_{B}. The calculated μ_{Fe} in FeSe and FeTe of 1.87 μ_{B} and 2.10 μ_{B} can be compared with the values of 2.01 μ_{B} and 2.16 μ_{B} from projector augmented wave calculations for the equivalent single stripe configuration [13]. The relaxation of the structures further suppresses these values to 0.95 μ_{B} and 1.39 μ_{B}, respectively. Our calculations indicate that μ_{Fe} is extremely sensitive to changes of a and u (and also c). DFT calculations of similar systems [12] have also shown sensitivity of the magnetic properties to the details of the structure, DFT methodology, and type of functional used.

The magnetic hyperfine field at the Fe nucleus reflects the s-electron polarization. We can distinguish a valence contribution to the total B_{hf} and a core contribution originating from the polarization of deep level s-electrons. In all systems, the core contribution is always larger in absolute value and of opposite sign with respect to the valence contribution to the total field. These two contributions cancel each other and give the values presented in Table 2.

The fact that Mössbauer spectroscopy shows no detectable B_{hf}, while the calculations predict sizable B_{hf} (between 1.3 and 15.6 T depending on the system and optimization scenario), can probably be explained by the strong itinerant nature of the spin fluctuations in this system.

4.2.3. Mössbauer Isomer Shifts and Electric Field Gradients

The measured Mössbauer isomer shift consists of the chemical shift (δ_{CS}) and the second order Doppler shift (δ_{SOD}). The sign of the δ_{SOD} is negative and vanishes at 0 K. Therefore, the chemical shift, δ_{SC}, is in fact the only

contribution to the isomer shift at 0 K.

Comparing the results of the calculations of the Mössbauer parameters with the available experimental results, we can see that the relatively low value of the principal component V_{zz} of the electric field gradient at Fe site is very well reproduced. Using the approximate formula, $EFG[10^{21}\ \mathrm{Vm}^{-2}] \approx 6\delta[\mathrm{mm/s}]$ [31], we can estimate the experimentally determined V_{zz}, as extracted from the measured quadrupole splitting.

The calculated V_{zz} = -0.49 $\times$ 10^{21} Vm^{-2} at Fe in FeS (LDA, optimized geometry, 0 K) can be compared with the measured room temperature (RT) values of 0.36(6) and 0.42(12) $\times$ 10^{21} Vm^{-2} (sign undetermined) [4, 7]. For FeSe and FeTe the calculated V_{zz} values after optimization are virtually identical (-0.62 $\times$ 10^{21} Vm^{-2}). This result can be compared with the available experimental data. The values for FeSe are in the range from 1.08 to 1.74 $\times$ 10^{21} Vm^{-2} obtained at RT [8, 9, 32–35] pointing towards EFG off-stoichiometry dependence. The relative errors of the cited experimental values are within (4 - 62)%. At lower temperatures, extracted values for V_{zz} are 1.722(6) $\times$ 10^{21} Vm^{-2} (120 K) [8], 1.80(12) $\times$ 10^{21} Vm^{-2} (80 K) [32] and 2.04(18) $\times$ 10^{21} Vm^{-2} (5 K) [32]. The temperature dependence of the quadrupole splitting for FeSe seems to be pretty flat [8, 32]. The extracted V_{zz} values for FeTe are in range from 1.53 to 1.92 $\times$ 10^{21} Vm^{-2} obtained at RT [9, 35–38]. The relative errors of the cited experimental values are within (2 - 53)%. For FeTe, it was found that the quadrupole splitting is increasing with decreasing temperature following $T^{3/2}$ power law [36].

With these relatively low absolute values, it is difficult to expect perfect agreement. The EFG remains low, but it does seem to be moderately sensitive to structural optimization (see Figure 3). The quadrupole splitting is essentially the same in a wide temperature range for FeSe and FeTe as found experimentally [32, 36]. The similar is found in our calculations. For all three investigated compounds, the *p*-*p* and *d*-*d* contributions to the EFG are of similar magnitude but of opposite sign. Because of their mutual cancellation, the V_{zz} values in these compounds are small. Also, the *p*-*f* contribution to the EFG at Fe site is almost

zero for FeTe and is increasing with lowering the atomic number of chalcogen atom. The discrepancy between the measured and calculated results could be partly explained by the fact that the investigated samples were off-stoichiometric with Fe in excess [32, 36] affecting the overall structure, particularly the local structure, and therefore the measured quadrupole splitting. Consequently, the off-stoichiometry present in the compound would shift the Fermi level. Since, the EFG is very sensitive to the density of states at the Fermi level, it is important to have insight into the anisotropy of p- and d-electron density at the Fermi level. For the $P4/nmm$ space group and the $2a$-Fe site with D_{2d}-point symmetry, the formulas for the p-, and d-anisotropy functions can be found in Ref. [17]. The p- and d-anisotropy functions for FeS have negligible slopes in the vicinity of the Fermi level. Therefore FeS-EFG is the least affected by the possible Fermi level shifts, e.g., by stoichiometry. The similar might be said for the slope of p-anisotropy close to the Fermi level for both FeSe and FeTe (0.04 states/eV). The slopes of the d-anisotropy function in the vicinity of the Fermi level for FeSe and FeTe are significant (≈ 2.5 and ≈ 2 states/eV, respectively), which in case of various off-stoichiometries could induce differences in the EFGs.

There is an unknown effect of the possibly present magnetic hyperfine field (out of the time scale of the Mössbauer measurements) on the quadrupole splitting measured in the experiment that could be an additional reason for the observed discrepancies between calculation and experiment.

The direction of the principal axis of the calculated EFG coincides with the z-axis of the crystal cell in all of the investigated systems. While the asymmetry parameter η equals to zero for the NM, FM, and AFM1 magnetic configurations, the ground state collinear AFM2 configuration breaks the axial symmetry, and η assumes non-zero values (Table 2). Mössbauer spectroscopy cannot measure η directly.

The calculated δ_{CS} of the Fe atom was obtained by contrasting the electron density at the Fe nucleus with the corresponding reference value of bcc α-Fe, as described in Ref. [18]. The calculated value of δ_{CS} in FeS is 0.45 mms^{-1}. The measured δ values of 0.373 - 0.44 mms^{-1} [7, 39, 40] are obtained at room

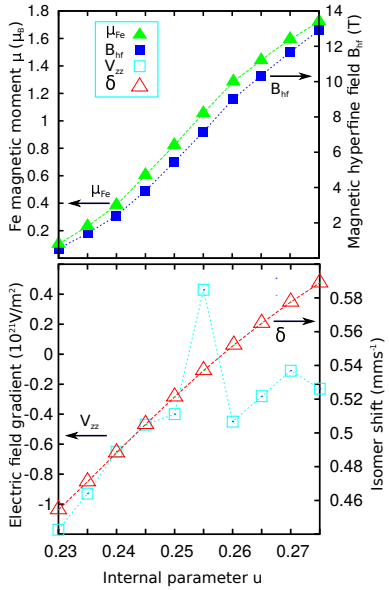

Figure 3: (Color online) Fe magnetic moment, magnetic hyperfine field, electric field gradient, and isomer shift as a function of the internal parameter u.

temperature (rel. errors (0.3 - 7)%), 0.53 mms^{-1} at 11 K [40], and $\approx$ 0.58 mms^{-1} at 1.7 K [39]. The $\delta_{\rm SOD}$ contribution is expected to decrease with decreasing temperature, with low $\delta_{\rm SOD}$ contribution at low temperatures. In general, the sensitivity of the density charge distribution on the compound off-stoichiometry could be the reason for the discrepancy of the experimentally and calculated chemical shift. Therefore, the calculated $\delta_{\rm CS}$ matches relatively well the measured ones.

Similarly to the V_{zz} parameters, the calculated $\delta_{\rm CS}$ values in FeSe and FeTe are again very close (0.54 and 0.56 mms^{-1}), which can be contrasted to the measured δ of 0.45 - 0.48 mms^{-1} (rel. errors within (0.4 - 38)%) obtained for both compounds at room temperature [8, 9, 32, 34–38]. Additionally, the measured δ at low temperatures are 0.5476(3) mms^{-1} (120 K) [8], 0.55(2) mms^{-1} (80 K) [32], and 0.59(3) mms^{-1} (5 K) [32] for tetragonal FeSe. Our calculated results matches very well the experimental ones.

While not exactly matching the experimental results, our calculations clearly

reproduce the experimental trends. One could, at least to a degree, expect an improvement in the agreement between the calculated and experimental HI parameters after performing a complete structural optimization along the z-axis, which would require going beyond the employed DFT scheme in this work.

4.2.4. The Influence of Anion Height

From our results one can see that small changes of u and a have a substantial effect on the calculated properties, and especially on μ_{Fe} and B_{hf}. To show this, in Figure 3 we present μ_{Fe}, B_{hf}, V_{zz}, and δ_{CS} in FeS as a function of u. The range of u was chosen in such a way as to span between the experimental and theoretically determined values and extend somewhat beyond these limits. It is clear that μ_{Fe} and B_{hf} exhibit drastic, albeit monotonic changes, whereas V_{zz}, and especially δ_{CS} are more stable with respect to changes of u. Even though V_{zz} changes sign, its absolute value is still relatively low. Similar plots can be produced for FeSe and FeTe as well. Because of this strong dependence on u, i.e., on the chalcogen atom height from the iron plane, the question of optimal optimization along the z-axis of the unit cell of these materials, currently difficult to perform within the DFT theory, becomes very important. The anion height has been shown to have strong correlation with the superconducting properties of the iron-based superconductors [41].

5. Bader analysis

The calculated Mössbauer parameters reflect the properties of the electronic charge density around the Fe ions. To obtain more information on the charge distribution between the atoms and to elucidate the type and topology of the chemical bonds, we employed the Bader's atoms in molecule theory [42], as implemented in the CRITIC2 code [43].

Table 3 gives the Bader analysis on the NM structures with experimental a, c, and u parameters within the LDA approximation.

As can be seen, Bader's theory predicts a sizable charge transfer from Fe to the chalcogen atom, with the largest amount of charge transferred in FeS.

Table 3: Bader charges and volumes of Fe and chalcogen atoms in FeX (X = S, Se, Te). The units are in a.u..

	Atom	Bader charge	Volume
FeS	Fe	25.41	80.0
	S	16.58	149.2
FeSe	Fe	25.56	88.4
	Se	34.43	176.5
FeTe	Fe	25.81	97.7
	Te	52.18	212.8

The volumes in Table 3 are defined as space enclosed by a zero flux surface of the gradient field of electron density, and the Bader charges are obtained by integrating the charge contained in these volumes. As the size of the cell and the interatomic distances are increased, the Bader volumes are increased too, while the transferred charge to the chalcogen atom is reduced. This also indicates a reduction of the polar character of the Fe-X bond.

The data related to the bond critical points in this system are presented in Table 4. In all three cases the Morse rule [42] for periodic systems was satisfied. Several different types of bonding critical points (*bcp*) were found: (1) between Fe and the NN chalcogen atom, (2) in the center of the unit cell connecting two chalcogen atoms from two different $x - y$ planes, and (3) between two in-plane Fe atoms in FeSe and FeTe. The latter *bcp* is missing in the FeS system, so in this compound two Fe atoms seem to be bonded only indirectly, via the S atoms.

The first type of *bcp* is positioned asymmetrically with respect to the center of the bond-path, closer to the iron ion. This asymmetry is more pronounced as we go down the sequence FeS→FeSe→FeTe. The other two types of *bcp* are found in the center of the corresponding bonds. As an example, the contour map representation of the charge density of FeS and the position of the critical points is given in Figure 4.

Table 4: Bond critical point (*bcp*) data in FeX (X = S, Se, Te). R1 is the distance along the bond path from the first atom to the *bcp*, while R2 is the distance from the *bcp* to the second atom. $\rho(bcp)$ and $\nabla^2\rho$ are the charge density and Laplacian at the critical point. The units are in a.u..

	Bond	R1	R2	R1/R2	$\rho(bcp)$	$\nabla^2\rho$
FeS	Fe-S	2.036	2.227	0.914	0.086	0.138
	S-S	3.351	3.351	1.000	0.008	0.023
FeSe	Fe-Se	2.126	2.397	0.887	0.072	0.096
	Fe-Fe	2.519	2.519	1.000	0.041	0.045
	Se-Se	3.502	3.502	1.000	0.008	0.019
FeTe	Fe-Te	2.203	2.702	0.815	0.061	0.014
	Fe-Fe	2.555	2.555	1.000	0.039	0.035
	Te-Te	3.665	3.665	1.000	0.010	0.017

The charge density at the *bpc*, $\rho(bcp)$, is a good indication of the type of the chemical bond. $\rho(bcp)$ larger than 0.2 would indicate covalent bonding. As we have $\rho(bcp) < 0.10$ in all cases, the bonds in this system are of closed-shell type [44]. This low density is what one would expect in a system with van der Waals type of interaction. This is also consistent with the positive value of the Laplacian, $\nabla^2\rho > 0$, indicating depletion of charge density along the bond path. The F-X *bpc* densities of decreasing intensity from Fe via FeSe to FeTe indicate closed-shell bonds of increasing magnitude.

6. Conclusion

Using first principles calculations, we have investigated the electronic and magnetic properties, hyperfine interactions parameters, and charge density of FeX (X = S, Se, Te). The magnetic ground state in all system has been found to be the anti-ferromagnetic collinear ordering. Even though only $Fe_{1+y}Te$ exhibits magnetic ordering at T > 0 K, there is a fair agreement between the available experimental data and the calculated values, especially considering the trends in the hyperfine interaction parameters across the investigated materials. The

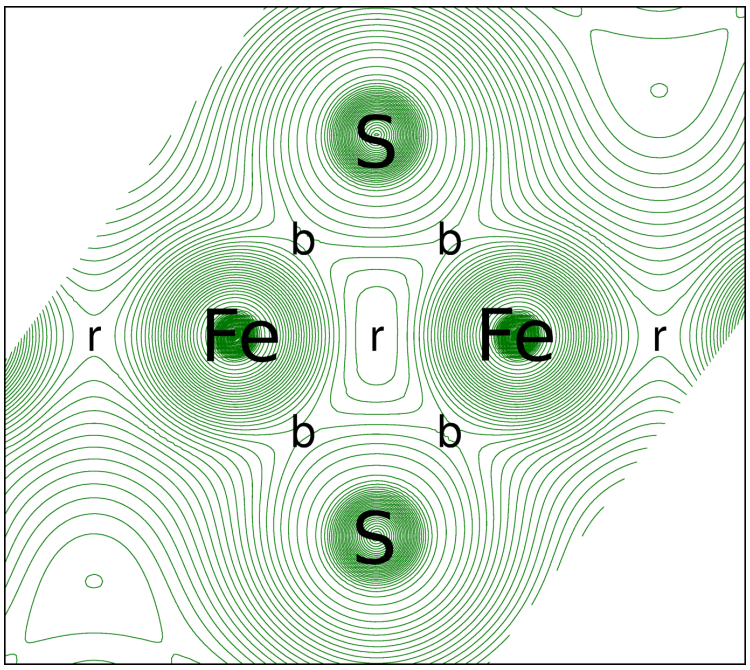

Figure 4: (Color online) Logarithmic contour map representation of the FeS charge density. The charge is presented in a plane connects two Fe atom with one NN Se atom above and another NN Se atom below the iron $x - y$ plane. b denotes bonding critical point, while r denotes ring critical point.

calculations predict finite hyperfine magnetic fields, which, due to the itinerant nature of the system cannot be detected in Mössbauer experiments. The low values of the quadruple splitting, as well as the trend in the isomer shift values are clearly reproduced. The Fe magnetic moments, hyperfine magnetic fields, electric field gradients, are found to be extremely sensitive to the fine details of the optimization, and critically depend on the anion height (parameter u), which cannot be accurately determined within the DFT formalism. By using Bader's atoms in molecule theory, the bonds in this system have been determined to be of closed-shell type. Our calculations indicate sizable charge transfer from the Fe to the chalcogen atoms.

Acknowledgement

We gratefully acknowledge the help of Dr. Cedomir Petrovic from Brookhaven National Laboratory, USA. This work has been supported by the grant No. 171001 from the Ministry of Education, Science and Technological Development of the Republic of Serbia.

References

[1] C. K. H. Borg, X. Zhou, C. Eckberg, D. J. Campbell, S. R. Saha, J. Paglione, E. E. Rodriguez, Strong anisotropy in nearly ideal tetrahedral superconducting FeS single crystals, Phys. Rev. B 93 (2016) 094522. doi:10.1103/PhysRevB.93.094522.
URL http://link.aps.org/doi/10.1103/PhysRevB.93.094522

[2] S. He, J. He, W. Zhang, L. Zhao, D. Liu, X. Liu, D. Mou, Y.-B. Ou, Q.-Y. Wang, Z. Li, L. Wang, Y. Peng, Y. Liu, C. Chen, L. Yu, G. Liu, X. Dong, J. Zhang, C. Chen, Z. Xu, X. Chen, X. Ma, Q. Xue, X. J. Zhou, Phase diagram and electronic indication of high-temperature superconductivity at 65 K in single-layer FeSe films, Nat Mater 12 (7) (2013) 605–610, letter. doi:10.1038/nmat3648.
URL http://dx.doi.org/10.1038/nmat3648

[3] L.-F. Zhang, V. F. Becerra, L. Covaci, M. V. Milošević, Electronic properties of emergent topological defects in chiral p-wave superconductivity, Phys. Rev. B 94 (2016) 024520. doi:10.1103/PhysRevB.94.024520.
URL http://link.aps.org/doi/10.1103/PhysRevB.94.024520

[4] S. Holenstein, U. Pachmayr, Z. Guguchia, S. Kamusella, R. Khasanov, A. Amato, C. Baines, H.-H. Klauss, E. Morenzoni, D. Johrendt, H. Luetkens, Coexistence of low-moment magnetism and superconductivity in tetragonal FeS and suppression of T_c under pressure, Phys. Rev. B 93 (2016) 140506. doi:10.1103/PhysRevB.93.140506.
URL http://link.aps.org/doi/10.1103/PhysRevB.93.140506

[5] M. A. Tanatar, A. E. Böhmer, E. I. Timmons, M. Schütt, G. Drachuck, V. Taufour, K. Kothapalli, A. Kreyssig, S. L. Bud'ko, P. C. Canfield, R. M. Fernandes, R. Prozorov, Origin of the Resistivity Anisotropy in the Nematic Phase of FeSe, Phys. Rev. Lett. 117 (2016) 127001. doi:10.1103/PhysRevLett.117.127001.
URL http://link.aps.org/doi/10.1103/PhysRevLett.117.127001

[6] K. Kothapalli, A. E. Böhmer, W. T. Jayasekara, B. G. Ueland, P. Das, A. Sapkota, V. Taufour, Y. Xiao, E. Alp, S. L. Bud'ko, P. C. Canfield, A. Kreyssig, A. I. Goldman, Strong cooperative coupling of pressure-induced magnetic order and nematicity in FeSe, Nature Communications 7 (2016) 12728. doi:10.1038/ncomms12728.
URL http://http://www.nature.com/articles/ncomms12728

[7] A. Wang, L. Wu, V. N. Ivanovski, J. B. Warren, J. Tian, Y. Zhu, C. Petrovic, Critical current density and vortex pinning in tetragonal $FeS_{1-x}Se_x$ ($x = 0,\ 0.06$), Phys. Rev. B 94 (2016) 094506. doi:10.1103/PhysRevB.94.094506.
URL http://link.aps.org/doi/10.1103/PhysRevB.94.094506

[8] A. Błachowski, K. Ruebenbauer, J. Żukrowski, J. Przewoźnik, K. Wojciechowski, Z. Stadnik, Mössbauer spectroscopy evidence for the lack of

iron magnetic moment in superconducting FeSe, Journal of Alloys and Compounds 494 (12) (2010) 1–4. doi:10.1016/j.jallcom.2009.12.095.
URL http://www.sciencedirect.com/science/article/pii/S0925838809026486

[9] R. W. Gómez, V. Marquina, J. L. Pérez-Mazariego, R. Escamilla, R. Escudero, M. Quintana, J. J. Hernández-Gómez, R. Ridaura, M. L. Marquina, Effects of Substituting Se with Te in the FeSe Compound: Structural, Magnetization and Mössbauer Studies, Journal of Superconductivity and Novel Magnetism 23 (4) (2010) 551–557. doi:10.1007/s10948-010-0764-2.
URL http://dx.doi.org/10.1007/s10948-010-0764-2

[10] D. C. Johnston, The puzzle of high temperature superconductivity in layered iron pnictides and chalcogenides, Advances in Physics 59 (6) (2010) 803–1061. arXiv:http://dx.doi.org/10.1080/00018732.2010.513480, doi:10.1080/00018732.2010.513480.
URL http://dx.doi.org/10.1080/00018732.2010.513480

[11] K. D. Kwon, K. Refson, S. Bone, R. Qiao, W.-l. Yang, Z. Liu, G. Sposito, Magnetic ordering in tetragonal FeS: Evidence for strong itinerant spin fluctuations, Phys. Rev. B 83 (2011) 064402. doi:10.1103/PhysRevB.83.064402.
URL http://link.aps.org/doi/10.1103/PhysRevB.83.064402

[12] I. I. Mazin, M. D. Johannes, L. Boeri, K. Koepernik, D. J. Singh, Problems with reconciling density functional theory calculations with experiment in ferropnictides, Phys. Rev. B 78 (2008) 085104. doi:10.1103/PhysRevB.78.085104.
URL http://link.aps.org/doi/10.1103/PhysRevB.78.085104

[13] H. Shi, Z.-B. Huang, J. S. Tse, H.-Q. Lin, Magnetic behavior of Fe(Se, Te) systems: First-principles calculations, Journal of Applied Physics 110 (4). doi:10.1063/1.3624759.

URL http://scitation.aip.org/content/aip/journal/jap/110/4/10.1063/1.3624759

[14] F. Ma, W. Ji, J. Hu, Z.-Y. Lu, T. Xiang, First-Principles Calculations of the Electronic Structure of Tetragonal α-FeTe and α-FeSe Crystals: Evidence for a Bicollinear Antiferromagnetic Order, Phys. Rev. Lett. 102 (2009) 177003. doi:10.1103/PhysRevLett.102.177003.
URL http://link.aps.org/doi/10.1103/PhysRevLett.102.177003

[15] P. Blaha, K. Schwarz, G. Madsen, D. Kvasnicka, J. Luitz, Wien2k, An Augmented Plane Wave + Local Orbitals Program for Calculating Crystal Properties, (Karlheinz Schwarz, Techn. Universität Wien, Austria) 2001. ISBN 3-9501031-1-2 (2001).

[16] K. Lejaeghere, G. Bihlmayer, T. Björkman, P. Blaha, S. Blügel, V. Blum, D. Caliste, I. E. Castelli, S. J. Clark, A. Dal Corso, S. de Gironcoli, T. Deutsch, J. K. Dewhurst, I. Di Marco, C. Draxl, M. Dułak, O. Eriksson, J. A. Flores-Livas, K. F. Garrity, L. Genovese, P. Giannozzi, M. Giantomassi, S. Goedecker, X. Gonze, O. Grånäs, E. K. U. Gross, A. Gulans, F. Gygi, D. R. Hamann, P. J. Hasnip, N. A. W. Holzwarth, D. Iuşan, D. B. Jochym, F. Jollet, D. Jones, G. Kresse, K. Koepernik, E. Küçükbenli, Y. O. Kvashnin, I. L. M. Locht, S. Lubeck, M. Marsman, N. Marzari, U. Nitzsche, L. Nordström, T. Ozaki, L. Paulatto, C. J. Pickard, W. Poelmans, M. I. J. Probert, K. Refson, M. Richter, G.-M. Rignanese, S. Saha, M. Scheffler, M. Schlipf, K. Schwarz, S. Sharma, F. Tavazza, P. Thunström, A. Tkatchenko, M. Torrent, D. Vanderbilt, M. J. van Setten, V. Van Speybroeck, J. M. Wills, J. R. Yates, G.-X. Zhang, S. Cottenier, Reproducibility in density functional theory calculations of solids, Science 351 (6280). arXiv:http://science.sciencemag.org/content/351/6280/aad3000.full.pdf, doi:10.1126/science.aad3000.
URL http://science.sciencemag.org/content/351/6280/aad3000

[17] K. Schwarz, C. Ambrosch-Draxl, P. Blaha, Charge distribution and electric-

field gradients in $YBa_2Cu_3O_{7-x}$, Phys. Rev. B 42 (1990) 2051–2061. doi:10.1103/PhysRevB.42.2051.
URL http://link.aps.org/doi/10.1103/PhysRevB.42.2051

[18] P. Blaha, Calculations of Mössbauer parameters in solids by DFT band-structure calculations, Journal of Physics: Conference Series 217 (1) (2010) 012009.
URL http://stacks.iop.org/1742-6596/217/i=1/a=012009

[19] T. Korhonen, A. Settels, N. Papanikolaou, R. Zeller, P. H. Dederichs, Lattice relaxations and hyperfine fields of heavy impurities in fe, Phys. Rev. B 62 (2000) 452–460. doi:10.1103/PhysRevB.62.452.
URL https://link.aps.org/doi/10.1103/PhysRevB.62.452

[20] S. Cottenier, H. Haas, Hyperfine fields and local lattice relaxation at $4d$ and $5sp$ impurities in bcc iron, Phys. Rev. B 62 (2000) 461–467. doi:10.1103/PhysRevB.62.461.
URL https://link.aps.org/doi/10.1103/PhysRevB.62.461

[21] J. P. Perdew, K. Burke, M. Ernzerhof, Generalized Gradient Approximation Made Simple, Phys. Rev. Lett. 77 (1996) 3865–3868. doi:10.1103/PhysRevLett.77.3865.
URL http://link.aps.org/doi/10.1103/PhysRevLett.77.3865

[22] P. Blaha, K. Schwarz, P. H. Dederichs, First-principles calculation of the electric-field gradient in hcp metals, Phys. Rev. B 37 (1988) 2792–2796. doi:10.1103/PhysRevB.37.2792.
URL http://link.aps.org/doi/10.1103/PhysRevB.37.2792

[23] A. Kokalj, XCrySDen—a new program for displaying crystalline structures and electron densities, Journal of Molecular Graphics and Modelling 17 (34) (1999) 176–179. doi:10.1016/S1093-3263(99)00028-5.
URL http://www.sciencedirect.com/science/article/pii/S1093326399000285

[24] T. Imai, K. Ahilan, F. L. Ning, T. M. McQueen, R. J. Cava, Why does undoped fese become a high-T_c superconductor under pressure?, Phys. Rev. Lett. 102 (2009) 177005. doi:10.1103/PhysRevLett.102.177005.
URL http://link.aps.org/doi/10.1103/PhysRevLett.102.177005

[25] Q. Wang, Y. Shen, B. Pan, Y. Hao, M. Ma, F. Zhou, P. Steffens, K. Schmalzl, T. R. Forrest, M. Abdel-Hafiez, X. Chen, D. A. Chareev, A. N. Vasiliev, P. Bourges, Y. Sidis, H. Cao, J. Zhao, Strong interplay between stripe spin fluctuations, nematicity and superconductivity in fese, Nat Mater 15 (2016) 159–163. doi:10.1038/nmat4492.
URL http://www.nature.com/nmat/journal/v15/n2/abs/nmat4492.html#supplementary-information

[26] W. Bao, Y. Qiu, Q. Huang, M. A. Green, P. Zajdel, M. R. Fitzsimmons, M. Zhernenkov, S. Chang, M. Fang, B. Qian, E. K. Vehstedt, J. Yang, H. M. Pham, L. Spinu, Z. Q. Mao, Tunable ($\delta\pi$, $\delta\pi$)-type antiferromagnetic order in α-fe(te,se) superconductors, Phys. Rev. Lett. 102 (2009) 247001. doi:10.1103/PhysRevLett.102.247001.
URL http://link.aps.org/doi/10.1103/PhysRevLett.102.247001

[27] E. E. Rodriguez, C. Stock, P. Zajdel, K. L. Krycka, C. F. Majkrzak, P. Zavalij, M. A. Green, Magnetic-crystallographic phase diagram of the superconducting parent compound $fe_{1+x}te$, Phys. Rev. B 84 (2011) 064403. doi:10.1103/PhysRevB.84.064403.
URL http://link.aps.org/doi/10.1103/PhysRevB.84.064403

[28] A. R. Lennie, S. A. T. Redfern, P. F. Schofield, D. J. Vaughan, Synthesis and Rietveld crystal structure refinement of mackinawite, tetragonal FeS, Mineralog. Mag. 59 (1995) 677–683.

[29] U. Pachmayr, N. Fehn, D. Johrendt, Structural transition and superconductivity in hydrothermally synthesized FeX (X = S, Se), Chem. Commun. 52 (2016) 194–197. doi:10.1039/C5CC07739G.
URL http://dx.doi.org/10.1039/C5CC07739G

[30] Y. Mizuguchi, F. Tomioka, S. Tsuda, T. Yamaguchi, Y. Takano, FeTe as a candidate material for new iron-based superconductor, Physica C: Superconductivity 469 (1520) (2009) 1027–1029, proceedings of the 21st International Symposium on Superconductivity (ISS 2008)Proceedings of the 21st International Symposium on Superconductivity (ISS 2008). doi:10.1016/j.physc.2009.05.177.
URL http://www.sciencedirect.com/science/article/pii/S0921453409002135

[31] H. M. Petrilli, P. E. Blöchl, P. Blaha, K. Schwarz, Electric-field-gradient calculations using the projector augmented wave method, Phys. Rev. B 57 (1998) 14690–14697. doi:10.1103/PhysRevB.57.14690.
URL http://link.aps.org/doi/10.1103/PhysRevB.57.14690

[32] T. M. McQueen, Q. Huang, V. Ksenofontov, C. Felser, Q. Xu, H. Zandbergen, Y. S. Hor, J. Allred, A. J. Williams, D. Qu, J. Checkelsky, N. P. Ong, R. J. Cava, Extreme sensitivity of superconductivity to stoichiometry in $Fe_{1+\delta}Se$, Phys. Rev. B 79 (2009) 014522. doi:10.1103/PhysRevB.79.014522.
URL http://link.aps.org/doi/10.1103/PhysRevB.79.014522

[33] T. M. McQueen, A. J. Williams, P. W. Stephens, J. Tao, Y. Zhu, V. Ksenofontov, F. Casper, C. Felser, R. J. Cava, Tetragonal-to-Orthorhombic Structural Phase Transition at 90 K in the Superconductor $Fe_{1.01}Se$, Phys. Rev. Lett. 103 (2009) 057002. doi:10.1103/PhysRevLett.103.057002.
URL http://link.aps.org/doi/10.1103/PhysRevLett.103.057002

[34] B. K. Jain, A. K. Singh, K. Chandra, An investigation of binary system $Fe - Se$, Journal of Physics F: Metal Physics 8 (12) (1978) 2625.
URL http://stacks.iop.org/0305-4608/8/i=12/a=021

[35] T. Tsuji, A. T. Howe, N. N. Greenwood, The $Fe - Se$ system. I. Mössbauer spectra and electrical conductivity of $Fe_{1.04}Se$, Journal of Solid State Chemistry 17 (1) (1976) 157–163. doi:http:

//dx.doi.org/10.1016/0022-4596(76)90216-4.
URL http://www.sciencedirect.com/science/article/pii/0022459676902164

[36] Z. M. Stadnik, P. Wang, J. Žukrowski, T. Noji, Y. Koike, A Mössbauer effect study of single crystals of the non-superconducting parent compound $Fe_{1.09}Te$ and the superconductor $FeSe_{0.4}Te_{0.6}$, Journal of Physics: Condensed Matter 25 (41) (2013) 416008.
URL http://stacks.iop.org/0953-8984/25/i=41/a=416008

[37] J. B. Ward, V. H. McCann, On the ^{57}Fe Mössbauer spectra of FeTe and Fe_2Te_3, Journal of Physics C: Solid State Physics 12 (5) (1979) 873.
URL http://stacks.iop.org/0022-3719/12/i=5/a=016

[38] J. Janaki, R. Govindaraj, T. G. Kumary, A. Mani, G. N. Rao, A. Bharathi, Synthesis, electrical transport and Mössbauer spectroscopy study of the layered iron tellurides $Fe_{1.1x}Ni_xTe$, physica status solidi (b) 249 (1) (2012) 134–137. doi:10.1002/pssb.201147275.
URL http://dx.doi.org/10.1002/pssb.201147275

[39] E. Bertaut, P. Burlet, J. Chappert, Sur l´absence d´ordre magnetique dans la forme quadratique de FeS, Solid State Communications 3 (10) (1965) 335–338. doi:http://dx.doi.org/10.1016/0038-1098(65)90090-6.
URL http://www.sciencedirect.com/science/article/pii/0038109865900906]

[40] M. Mullet, S. Boursiquot, M. Abdelmoula, J.-M. Génin, J.-J. Ehrhardt, Surface chemistry and structural properties of mackinawite prepared by reaction of sulfide ions with metallic iron, Geochimica et Cosmochimica Acta 66 (5) (2002) 829–836. doi:10.1016/S0016-7037(01)00805-5.
URL http://www.sciencedirect.com/science/article/pii/S0016703701008055

[41] Y. Mizuguchi, Y. Hara, K. Deguchi, S. Tsuda, T. Yamaguchi, K. Takeda, H. Kotegawa, H. Tou, Y. Takano, Anion height dependence of T_c for the

Fe-based superconductor, Superconductor Science and Technology 23 (5) (2010) 054013.
URL http://stacks.iop.org/0953-2048/23/i=5/a=054013

[42] R. F. W. Bader, Atoms in Molecules: A Quantum Theory, Oxford University Press, Oxford, 1990.

[43] A. O. de-la Roza, E. R. Johnson, V. Luaña, Critic2: A program for real-space analysis of quantum chemical interactions in solids, Computer Physics Communications 185 (3) (2014) 1007–1018. doi:10.1016/j.cpc.2013.10.026.
URL http://www.sciencedirect.com/science/article/pii/S0010465513003718

[44] C. F. Matta, R. J. Boyd, An Introduction to the Quantum Theory of Atoms in Molecules, Wiley-VCH Verlag GmbH & Co. KGaA, 2007, Ch. 1, pp. 1–34. doi:10.1002/9783527610709.ch1.
URL http://dx.doi.org/10.1002/9783527610709.ch1